Communication

Wideband High-Efficiency Circularly Polarized SIW-Fed S-Dipole Array for Millimeter-Wave Applications

Long Zhang, Ke Wu, Sai-Wai Wong, Yejun He, Peng Chu, Wenting Li, Kai Xu Wang, and Steven Gao

***Abstract*— A wideband high-efficiency millimeter-wave (mm-wave) circularly polarized (CP) array which is constituted by novel planar substrate integrated waveguide (SIW)-fed S-dipoles is presented in this communication. The proposed mm-wave CP S-dipole consists of two rotational symmetric curved arms and is fed differentially through aperture coupling, which features simple configuration and excellent performance. Detailed analysis is given to explain the operating principles of this element. It is noted that superior element performance including a wide impedance bandwidth of 43%, a wide 3 dB axial ratio (AR) bandwidth of 36%, and 1 dB gain bandwidth of 38% is achieved by the planar SIW-fed S-dipole. By feeding 64 in-phase S-dipole elements through a full-corporate SIW feeding network, a planar wideband highly efficient mm-wave 8 × 8 CP array is realized. To verify the design concept, a prototype operating at Ka-band is fabricated and measured. The measurement results indicate that the proposed array achieves a wide overlapped bandwidth of 27.6%, a high antenna gain of 25.2 dBic, and a high aperture efficiency of 89.9%. Attributed to the planar and robust array structure as well as its excellent performance, the presented array is a good candidate for various mm-wave applications.**

***Index Terms*— Circular polarization, millimeter wave (mm-wave), S-dipole, substrate integrated waveguide (SIW), wideband array.**

I. Introduction

Millimeter-wave (mm-wave) spectrum has received considerable interests with the rapid development of 5G mobile communications [1]. Although unprecedented spectrum resources can be harvested at mm-wave bands, signal attenuation becomes much more severe at these frequencies [2]. To cope with this issue, high-efficiency and high-gain mm-wave antennas need to be deployed [3].

With the sharp decrease in wavelength at mm-wave frequencies, dielectric loss, radiation loss, and metallic loss of transmission lines are no longer negligible [4]. Substrate integrated waveguide (SIW), which features low transmission loss and planar structure, is, thus, extensively employed to design high-efficiency and high-gain antennas [5].

Manuscript received November 17, 2018; revised July 31, 2019; accepted August 25, 2019. Date of publication September 16, 2019; date of current version March 3, 2020. This work was supported in part by the National Natural Science Foundation of China under Grant 61801299 and Grant 61372077, in part by the Consortium for Aerospace Research and Innovation in Canada (CARIC) and Natural Sciences and Engineering Research Council (NSERC) of Canada, and in part by the Shenzhen University Research Startup Project of New Staff under Grant 2019117. *(Corresponding author: Yejun He.)*

L. Zhang, S.-W. Wong, and Y. He are with the College of Electronics and Information Engineering, Shenzhen University, Shenzhen 518060, China (e-mail: long.zhang@szu.edu.cn; heyejun@126.com).

K. Wu is with the Department of Electrical Engineering, Poly-Grames Research Center, Polytechnique Montréal, Montreal, QC H3T 1J4, Canada (e-mail: ke.wu@polymtl.ca).

P. Chu is with the College of Electronic and Optical Engineering, Nanjing University of Posts and Telecommunications, Nanjing 210023, China.

W. Li and S. Gao are with the School of Engineering and Digital Arts, University of Kent, Canterbury CT2 7NT, U.K. (e-mail: s.gao@kent.ac.uk).

K. X. Wang is with the State Key Laboratory of Millimeter Waves, Department of Electronic Engineering, City University of Hong Kong, Hong Kong.

Color versions of one or more of the figures in this communication are available online at http://ieeexplore.ieee.org.

Digital Object Identifier 10.1109/TAP.2019.2940468

As is well known, circularly polarized (CP) antennas have several advantages such as the mitigation of multi-path fading, immunity of "Faraday rotation," and the reduction of polarization mismatching [6]. Attracted by these superior features, various mm-wave CP antenna elements based on the SIW technology were investigated, including the cavity-backed L-shaped patch [7], cavity-backed slot antenna [8], dual-CP planar aperture antenna [9], endfire complementary source antenna [10], and magnetoelectric (ME) dipole [11]. Although the aforementioned mm-wave elements effectively achieved CP radiation, they were not fully applicable for the implementation of wideband planar CP arrays due to their complicated structure, large size in excess of one wavelength, or the relatively narrower bandwidth.

Due to the limitation of waveguide cutoff frequency and the less flexibility of SIW compared to traditional transmission lines, the bandwidth of mm-wave SIW CP arrays are generally inferior to those mm-wave arrays fed by conventional transmission lines [12]–[14]. Recently, much effort has been devoted to improve the bandwidth of the SIW based large-scale CP arrays. In [15]–[17], ME dipole and spiral elements were utilized to implement wideband mm-wave SIW CP arrays, which achieved less than 20% bandwidth. Further improvement of bandwidth was realized by using the stacked patch and SIW sequential-rotation (SR) feeding network [18]. However, the SIW SR feeding network complicated the array design and increased the size of mm-wave array, which resulted in low array efficiency. In [19], a stacked curl element was used to constitute an mm-wave CP array, which realized an overlapped bandwidth of 30%. Nevertheless, additional substrate and vias were utilized to construct the stacked curl configuration, which imposed more stringent requirement on fabrication accuracy and increased the manufacture complexity.

In this communication, a novel planar SIW aperture-coupled CP S-dipole element is proposed for implementing large-scale mm-wave arrays. The presented element is excited differentially by aperture coupling without integrating any vias in the radiator. It features wide bandwidth and simple configuration, which is superior to other reported CP elements designed for large-scale mm-wave arrays. By exciting 64 mm-wave S-dipole elements in phase through an SIW full-corporate feeding network, a planar wideband highly efficient mm-wave 8 × 8 CP array is constructed and investigated. The measurement results indicate that the proposed array achieves wide overlapped bandwidth, high antenna gain, and high aperture efficiency.

II. MM-Wave SIW Aperture-Coupled S-Dipole Element

A. Element Geometry

The geometry of the proposed SIW aperture-coupled S-dipole element is shown in Fig. 1. As shown in Fig. 1(a) and (b), the S-dipole element is printed on the top layer of a Rogers RO5880 substrate with a dielectric constant of 2.2 and a loss tangent of 0.0009, which is constituted by two rotational symmetric curved arms with a gap of g. The thickness of the metal layer (copper) is 35 μm, while its conductivity is around 5.8×10^7 S/m. Each curved arm can be

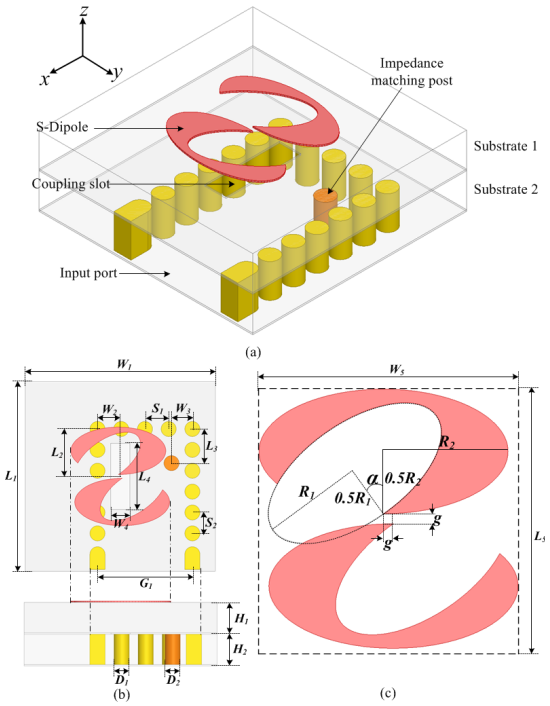

Fig. 1. Geometry of the proposed element with detailed dimensions. (a) Perspective view. (b) Top view and side view. (c) S-dipole.

TABLE I
ELEMENT DIMENSIONS (mm)

L_1	L_2	L_3	L_4	L_5	W_1	W_2	W_3	W_4	W_5
10	2.5	1.8	3.5	5.2	10	1.2	1.1	1	5.2
S_1	S_2	G_1	D_1	D_2	H_1	H_2	R_1	R_2	g
1.25	1.1	5	0.8	0.8	1.575	1.575	2	2.5	0.2

formed by subtracting a rotated smaller ellipse from a bigger ellipse as shown in Fig. 1(c). A rectangular slot is etched on the top layer of substrate 2 (Rogers RO5880) for energy coupling between the SIW and S-dipole element. To feed the element, an input port is placed in front of the SIW. Since the size of the rectangular slot controls the energy coupling factor, geometry parameters W_4 and L_4 can be used to tune the performance of the element. Besides, a copper post with diameter D_2 is positioned alongside the coupling slot, which helps achieve good impedance matching.

Table I gives the detailed geometry dimensions of the proposed mm-wave S-dipole element and the rotation angle α is 35°. It is worth pointing out that although an S-shaped antenna working at low frequencies was presented in [20], the proposed mm-wave S-dipole element is different and has novel advantages compared to the previous design in the following aspects.

1) The presented antenna in [20] is fed by a rather complicated microstrip balun, which brings a vertical transition from the microstrip line to the antenna. The nonplanar interlaced configuration between the antenna and the balun is hardly to be implemented at mm-wave bands. However, the mm-wave S-dipole proposed here is excited differentially through aperture coupling with fully planar structure, which is easy to be fabricated at mm-wave frequencies.
2) The proposed mm-wave S-dipole element can be readily used to constitute a large-scale mm-wave planar array, while the antenna presented in [20] is difficult to be extended to planar arrays.

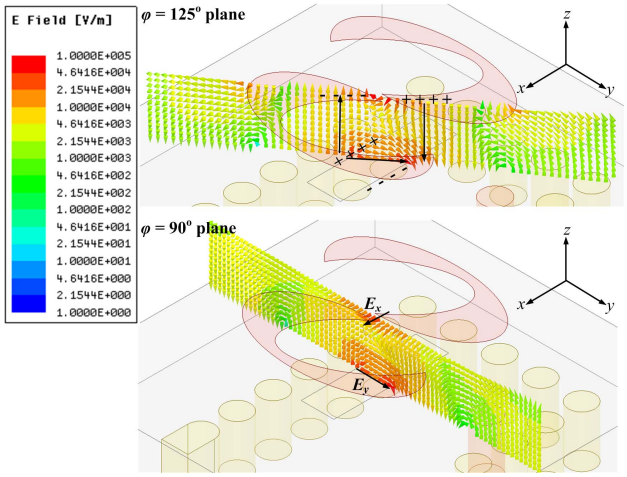

Fig. 2. Electric fields between the S-dipole element and the slot at 30 GHz.

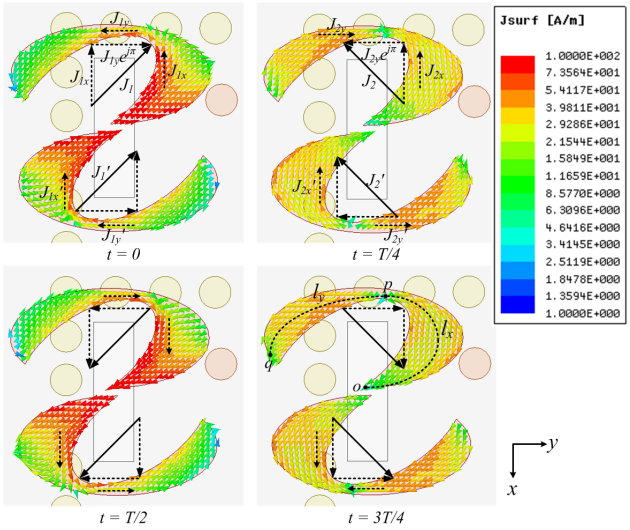

Fig. 3. Surface current distribution on the S-dipole element at 30 GHz.

3) The proposed element is fed by the SIW which has much lower transmission loss than the microstrip line used in [20]. Moreover, no direct connection between the SIW and the element is utilized, which benefits the antenna fabrication at mm-wave bands. By using aperture coupling, no vias or external circuit are needed to excite the antenna, which also improves the robustness of the proposed element.

B. Element-Operating Principles

As aforementioned, the S-dipole element is excited by the SIW through the EM coupling from the slot to the element. To explain the aperture coupling mechanism, Fig. 2 shows the electric fields between the element and the slot in two different planes which are perpendicular to the substrate. As is well known, the direction of electric fields across the waveguide broad-wall slot is perpendicular to long side of the slot, i.e., in the y-direction in Fig. 2. At the feeding area, it is designed that the two arms of the S-dipole element are placed at the opposite side of the slot, thus the coupling electric fields to the two arms are in the reverse direction, as shown by the electric fields distribution in the $\varphi = 125°$ plane. This coupling scheme yields an electric potential difference between the two arms, which makes the element excited differentially like a dipole.

Fig. 3 shows the surface current distribution on the S-dipole at four different states ($t = 0$, $T/4$, $T/2$, $3T/4$, where T is the period

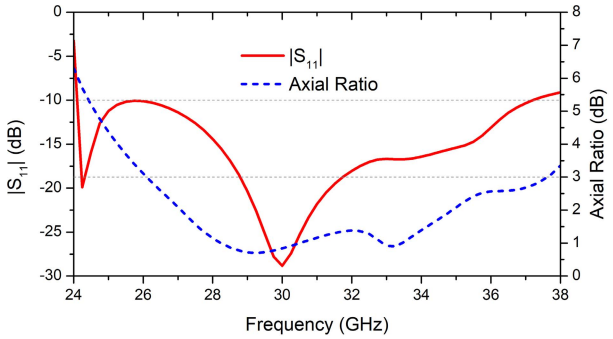

Fig. 4. Simulated $|S_{11}|$ and AR of the proposed S-dipole element.

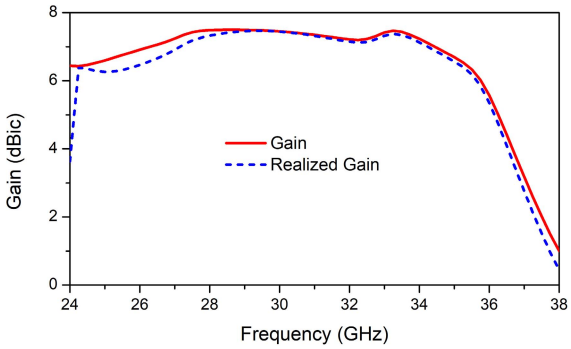

Fig. 5. Simulated gain and realized gain of the proposed S-dipole element.

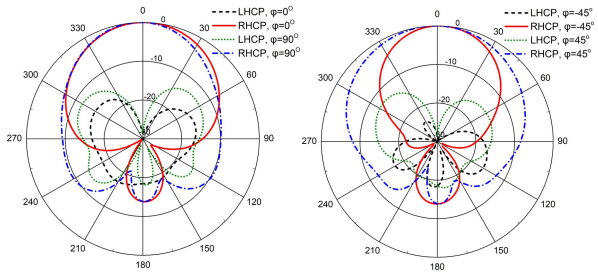

Fig. 6. Radiation patterns of the proposed S-dipole element at 30 GHz.

of time). As shown, the surface current on each S-dipole arm is roughly represented by two parts, i.e., the x-direction component $\vec{J}_x$ and y-direction component $\vec{J}_y$, and thus, the surface current on each arm can be obtained by the vector superposition of $\vec{J}_x$ and $\vec{J}_y$.

When $t = 0$, the surface current on the upper arm of the S-dipole can be calculated by

$$\vec{J}_1 = \vec{J}_{1x} + \vec{J}_{1y} \cdot e^{j\pi}. \tag{1}$$

The term $e^{j\pi}$ is introduced due to the fact that the phase of $\vec{J}_{1y}$ lags behind $\vec{J}_{1x}$ by π. Since the distance between the two phase centers of $\vec{J}_x$ and $\vec{J}_y$ is $(l_x + l_y)/2$, the phase difference between $\vec{J}_x$ and $\vec{J}_y$ is $\pi(l_x + l_y)/\lambda_g$, where λ_g is the guided wavelength in the substrate, and l_x and l_y represent the flowing path length of the electric current $\vec{J}_x$ and $\vec{J}_y$, respectively. The guided wavelength $\lambda_g$is calculated by $\lambda_0/\sqrt{\varepsilon}_{eff}$, where ε_{eff} is around 1.95 at 30 GHz. Since $l_x + l_y$ is about 7 mm which approaches to one λ_g at 30 GHz, the phase difference between $\vec{J}_{1x}$ and $\vec{J}_{1y}$ is around π.

As the two arms are rotationally symmetric and the element is feed differentially like a dipole, the surface current on the other arm of the S-dipole can be represented by

$$\vec{J}_1' = \vec{J}_{1x}' + \vec{J}_{1y}' \cdot e^{j\pi} = \vec{J}_1. \tag{2}$$

Likewise, when $t = T/4$, the surface current on the S-dipole can be calculated by

$$\vec{J}_2 = \vec{J}_{2x} + \vec{J}_{2y} \cdot e^{j\pi} = \vec{J}_2'. \tag{3}$$

Notice that $\vec{J}_2$ is lagging $\pi/2$ behind $\vec{J}_1$ due to the time delay of $T/4$, and the radiated electric fields of the S-dipole in the far-field can be calculated by using the vector potential $\vec{A}$

$$\vec{E} = -j\omega\vec{A} = -\frac{j\omega\mu}{4\pi}\iiint_V \left(\vec{J}_1 + \vec{J}_2 e^{j\pi/2}\right)\frac{e^{-jkR}}{R}dv \tag{4}$$

where R is the distance from any point on the element to the observation point. By designing the S-dipole element properly, it is able to make $\vec{J}_1$ and $\vec{J}_2$ perpendicular to each other and also possible to keep a good magnitude balance between the two orthogonal electric currents. Once these two conditions are attained, the S-dipole radiates CP waves in the far-field. Fig. 3 verifies that a right-hand circularly polarized (RHCP) wave is generated by the proposed S-dipole element.

C. Element Performance and Comparison With Other Planar Wideband MM-Wave CP Elements

The simulated reflection coefficient and axial ratio (AR) of the proposed element are shown in Fig. 4. As shown, the impedance bandwidth of the element is from 24.1 to 37.3 GHz (43%), while the AR bandwidth is from 26.1 to 37.6 GHz (36.1%). It is also observed from Fig. 4 that the proposed element has three resonances at 24.5, 30, and 35.5 GHz. By investigating the surface current on the element arm, it is indicated that the proposed element operates at quasi-0.75λ, quasi-1λ, and quasi-1.25λ modes at these three frequencies. Due to this multi-resonance feature, the proposed element can operate over a wide frequency range.

TABLE II

COMPARISON BETWEEN THE PROPOSED ELEMENT AND OTHER PLANAR WIDEBAND MM-WAVE CP ANTENNA ELEMENTS

Ref	Element Type	No. of Layers	Impedance BW	AR BW	Gain BW
[13]	Helical antenna	8	35.9%	34.1%	n. a.
[14]	Slot with patch	1	n. a.	21.2%	n. a.
[15]	ME-dipole	1	28.8%	25.9%	n. a.
[16]	Spiral	1	23%	21.9%	n. a.
[17]	Spiral	1	23.3%	17.5%	n. a.
[18]	Stacked patch	2	~26%	~17.5%	n. a.
[19]	Stacked curl	2	35.7%	39.5%	~34% (3 dB)
This Work	S-dipole	1	43%	36.1%	38% (1 dB)

Fig. 5 shows the simulated gain and realized gain of the proposed element. As shown, the element achieves a rather flat gain performance within the operating bandwidth. The peak gain is around 7.5 dBic, while the 1 dB gain bandwidth is roughly from 24 to 35.4 GHz (38%). The radiation patterns of the proposed element in different planes at 30 GHz are shown in Fig. 6. As shown, the element effectively radiates RHCP waves in the upper hemisphere region with nearly identical beamwidth in the two main planes, which makes the proposed element suitable for planar array application.

To demonstrate the advantages of the proposed mm-wave S-dipole element, Table II gives a comparison between the proposed element and other reported planar wideband mm-wave CP elements. As shown, the proposed element has much better performance than the

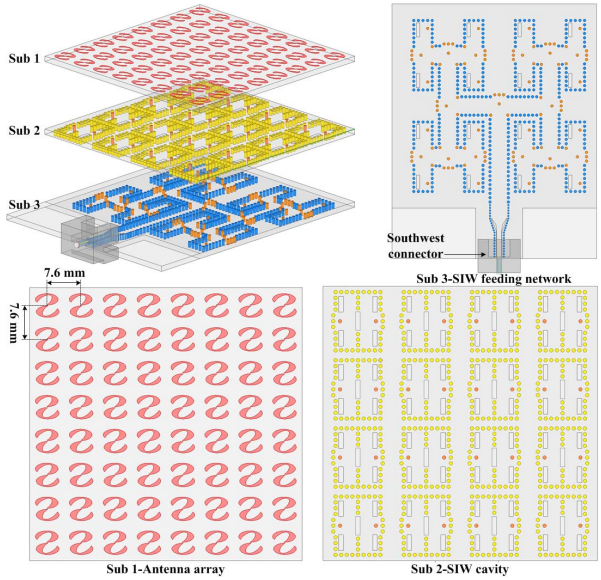

Fig. 7. Geometry of the proposed 8×8 wideband mm-wave SIW-fed array.

TABLE III
SIW CAVITY AND H-JUNCTION DIMENSIONS (mm)

L_6	L_7	L_8	L_9	W_6	W_7	W_8	W_9
4.2	2.7	2.4	2.8	1	1.2	1.35	1.25
S_3	S_4	S_5	d_1	d_2	d_3	d_4	d_5
1.2	1.3	1.375	0.5	1.5	0.6	2.75	5.1

mm-wave CP elements presented by the very recent research works [14]–[18].

Compared with the elements presented in [13] and [19], the proposed S-dipole has wider impedance bandwidth and gain bandwidth. More importantly, the proposed element can be printed on a single-layer substrate without integrating any vias in the radiator, which greatly reduces the fabrication complexity and improves the robustness.

III. MM-WAVE SIW-FED CP ARRAY DESIGN AND ANALYSIS

A. 8×8 Array Geometry

By employing the proposed wideband mm-wave S-dipole element, a planar 8×8 wideband mm-wave array is implemented which is shown in Fig. 7. As shown, three Rogers RO5880 substrates, each with a thickness of 1.575 mm, are sandwiched together to construct a full-corporate-fed mm-wave array. On the first substrate, 64 S-dipole elements are printed with an element space of 7.6 mm. To feed each element uniformly, 16 SIW cavities are placed underneath the S-dipole elements. Within each SIW cavity, four slots are carved at the four corners of the SIW cavity, while a longer slot is etched at the center of the cavity. The four peripheral slots are printed on the top layer of the second substrate, while the center slot is printed on the bottom layer. With this configuration, EM energy is coupled to the SIW cavity from the SIW feeding network through each center slot and then transmitted to the array elements through each peripheral slot. The 1 to 16 SIW power divider feeding network is constructed on the third substrate, which includes several SIW T-junctions, H-junctions, and a grounded coplanar waveguide (GCPW) to SIW transition. At the input port of the SIW feeding network, a southwest connector is utilized for measurement purpose.

Fig. 8 provides the geometry dimensions of the SIW cavity and the H-junction. A part of the geometry dimension values is already given in Table II and the remaining dimension values are given in Table III.

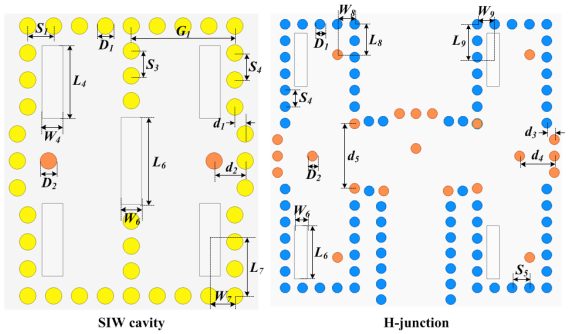

Fig. 8. Geometry dimensions of the SIW cavity and H-junction.

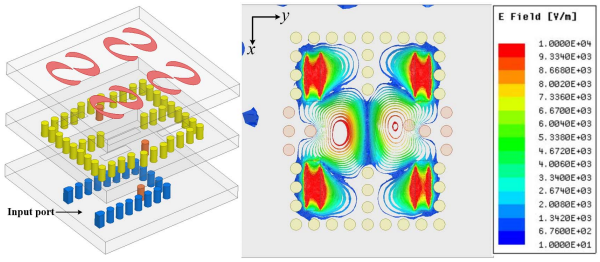

Fig. 9. 2×2 subarray. (a) Exploded view. (b) E-fields in the SIW cavity.

The dimensions of the coupling slot (W_4, L_4, W_6, and L_6) affect the S_{11} and AR of the proposed array, while the position of the posts (d_1, d_2, d_3, d_4, W_8, and L_8) mainly affects the impedance matching of the proposed array. Besides, the GCPW to the SIW transition also influences the S_{11} of the proposed array and should be elaborately designed.

B. 2×2 Subarray

The proposed 8×8 array is implemented by feeding sixteen 2×2 subarrays corporately. Each subarray is excited by an SIW cavity and it is designed that the four elements of the subarray is excited in phase.

Fig. 9(a) shows the configuration of the 2×2 subarray, while the E-fields in the SIW cavity are demonstrated in Fig. 9(b). As can be seen from Fig. 9(b), a quasi-TM^z_{320} mode is excited in the SIW cavity, which indicates a TM to z-direction mode. By etching four symmetric slots at the corners of the cavity, the four S-dipole elements can be excited in phase. Good impedance matching can be achieved by tuning the size and position of each slot as well as the position of the impedance matching post. The mutual coupling between each element can be alleviated by changing the coupling slot position, optimizing the geometry of the SIW cavity, and rearranging the impedance matching posts.

IV. RESULTS AND DISCUSSION

A. Prototype and Results

The fabricated prototype of the proposed 8×8 array is shown in Fig. 10. The three Rogers RO5880 substrates are stacked together by using a 0.003 in (0.076 mm)-thick Rogers CuClad 6700 bonding film, which has a dielectric constant of 2.30 and a loss tangent of 0.0025. The actual thickness of the bonding film is around 0.05 mm or thinner after laminating due to the pressure and heat. In such circumstances, the array performance slightly varies. On the bottom substrate, an extension board is designed to mount the southwest connector.

Fig. 11 shows the simulated and measured reflection coefficients of the proposed wideband mm-wave CP array. As shown, the measured

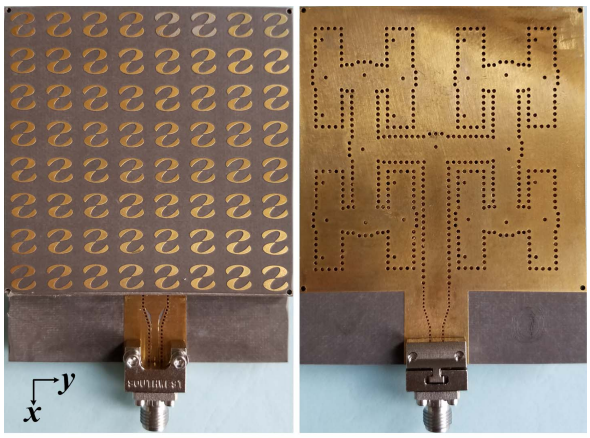

(a) (b)

Fig. 10. Fabricated prototype of the proposed 8×8 SIW-fed CP array. (a) Top view. (b) Bottom view.

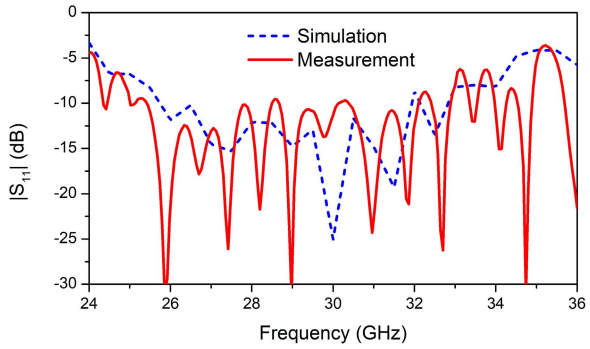

Fig. 11. Simulated and measured $|S_{11}|$ of the proposed array.

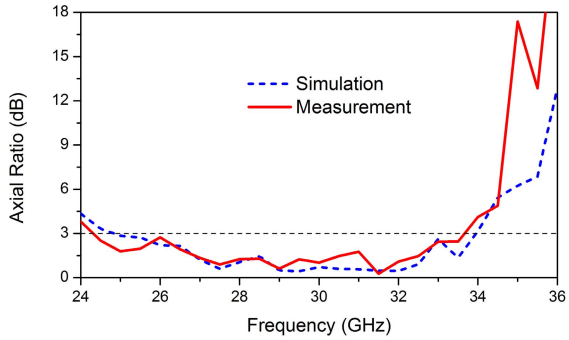

Fig. 12. Simulated and measured AR of the proposed array.

impedance bandwidth is from 25 to 33 GHz, equaling to a fractional bandwidth of 27.6%.

The radiation performance of the fabricated array is measured by an NSI-2000 near-field measurement system. The simulated and measured ARs are demonstrated in Fig. 12. As shown, the simulated 3 dB AR bandwidth is from 24.7 to 34 GHz (31.7%), while the measured 3 dB AR bandwidth is from 24.3 to 33.8 GHz (32.7%).

Fig. 13 shows the simulated and measured gains of the proposed array. The measurement gain of the proposed array was obtained by comparison with a standard gain horn. As shown, the measured peak gain is 25.18 dBic at 29 GHz, while the measured 3 dB gain bandwidth is from 24.3 to 32.8 GHz (30%). The peak aperture efficiency (ε_a) calculated by the measured gain is 89.9% at 26 GHz (measured gain is 25.02 dBic at 26 GHz and the aperture size is 61.2 mm × 61.2 mm), while the peak overall efficiency (aperture efficiency × radiation efficiency, $\varepsilon_a \times \varepsilon_{rad}$) is 75.2%.

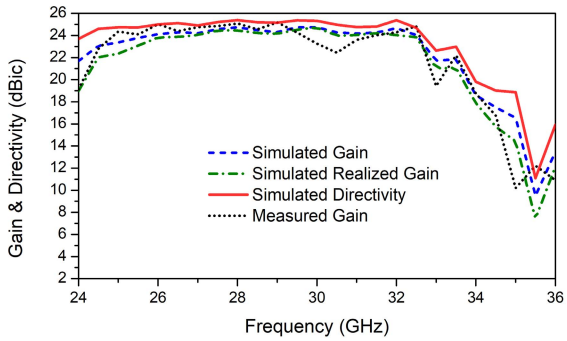

Fig. 13. Simulated and measured gain and directivity of the proposed array.

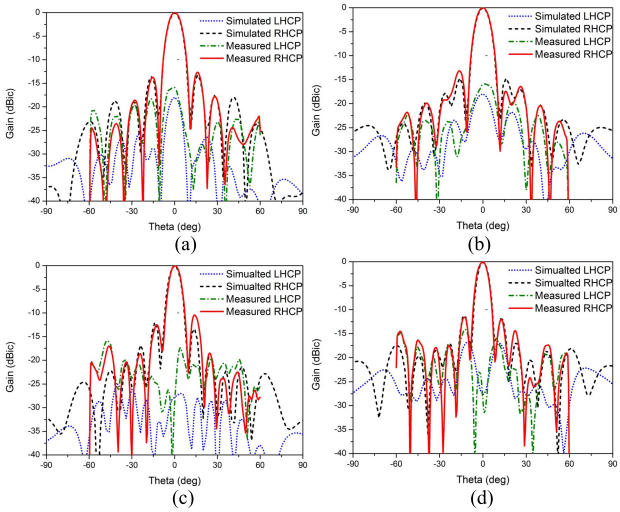

Fig. 14. Simulated and measured radiation patterns of the proposed array. (a) *xz* plane at 26 GHz. (b) *yz* plane at 26 GHz. (c) *xz* plane at 30 GHz. (d) *yz* plane at 30 GHz.

From Figs. 11–13, it is observed that the measurement results are better than the simulated results in the low frequency range (around 24.5–26.5 GHz) and worse than the simulated results around 30 GHz. These discrepancies may be caused by the fabrication and measurement errors. Moreover, the size of the ground plane affects the gain of the proposed element and array to a certain degree. Different ground plane size may result in maximum gain difference between the array and the element close to the gain of the array factor.

The simulated and measured radiation patterns at 26 and 30 GHz are shown in Fig. 14. Good agreement between the simulated results and measured results is observed. Unidirectional beams with around −15 dB sidelobe are achieved within the operating bandwidth.

B. Comparison and Discussion

A comparison between the proposed array and other reported planar wideband mm-wave CP arrays in terms of array configuration, operating frequency, impedance bandwidth, AR bandwidth, 3 dB gain bandwidth, peak gain, and peak efficiency is listed in Table IV. As can be seen from Table IV, majority of the recent research work achieves an overall bandwidth of less than 20%, while the proposed work can realize an overall bandwidth of 27.6%. Although the array presented in [19] achieves an overall bandwidth of 30.6%, the proposed SIW-fed S-dipole array has 1.7 dB higher antenna peak gain and a high aperture efficiency of 89.9%.

More importantly, the proposed array has a simpler configuration, more robust array structure, and is more cost-effective than the array

TABLE IV
COMPARISON BETWEEN THE PROPOSED ARRAY AND OTHER REPORTED WIDEBAND MM-WAVE CP ARRAYS

Ref.	Element Type	Fab. Tech.	No. of Substrate Layers	No. of Elements	Frequency (GHz)	Feeding Network	Impedance BW (%)	AR BW (%)	Gain BW (%)	Overall BW (%)	Peak Gain (dBic)	Peak Efficiency (%)
[13]	Helical antenna	LTCC	10	4 × 4	60	Full corporate	22	20	15.1	15.1	15.2	54.9 ($\varepsilon_a \times \varepsilon_{rad}$)
[14]	Slot with patch	PCB	4	4 × 4	28	Full corporate	28.6	14	n. a.	14	18.2	~65 ($\varepsilon_a \times \varepsilon_{rad}$)
[15]	ME dipole	PCB	3	8 × 8	60	Full corporate	18.2	16.5	18.2	16.5	26.1	72.2 ($\varepsilon_a \times \varepsilon_{rad}$)
[16]	Spiral	PCB	3	4 × 4	60	Sequential	14.1	21.1	16.4	14.1	19.5	87 (ε_{rad})
[17]	Spiral	PCB	3	4 × 4	60	Sequential	16.1	18.8	~20	16.1	20	52.4 (ε_a)
[18]	Stacked patch	PCB	2	4 × 4	29	Sequential	29.6	25.4	19	19	20.3	>57.9 (ε_{rad})
[19]	Stacked curl	PCB	4	8 × 8	37.5	Full corporate	35.4	33.8	32.2	30.6	23.5	77.8 ($\varepsilon_a \times \varepsilon_{rad}$)
This Work	S-dipole	PCB	3	8 × 8	30	Full corporate	27.6	32.7	30	27.6	25.2	89.9 (ε_a) 75.2 ($\varepsilon_a \times \varepsilon_{rad}$)

presented in [19] due to the following reasons. First, only three substrates are utilized in the proposed array, while the array in [19] stacks four substrates. Besides, no via is required in the radiator for the proposed design, which avoids drilling considerable blind vias and, thus, greatly reduces the fabrication complexity and cost. Moreover, array elements in the proposed design are unilaterally printed on the substrate without integrating any via, which alleviates the requirement of high fabrication accuracy at mm-wave frequencies and yields a more robust array structure.

V. CONCLUSION

A planar wideband high-efficiency CP array based on a novel SIW-fed S-dipole has been proposed. By exciting the mm-wave S-dipole differentially through aperture coupling, good CP radiation is realized. Attributed to the multi-resonance characteristic of the proposed element, a wide impedance bandwidth of 43%, a wide 3 dB AR bandwidth of 36%, and a 1 dB gain bandwidth of 38% have been achieved. Through feeding the wideband mm-wave S-dipole elements by a full-corporate SIW feeding network, a planar 8×8 SIW CP array is designed, fabricated, and measured. Excellent bandwidth performance and high aperture efficiency have been achieved. Due to the planar and robust configuration, wide bandwidth, and high efficiency, the proposed array would be a promising candidate for various mm-wave applications.

REFERENCES

[1] T. Rappaport, Y. Xing, G. R. MacCartney, A. F. Molisch, E. Mellios, and J. Zhang, "Overview of millimeter wave communications for fifth-generation (5G) wireless networks-with a focus on propagation models," *IEEE Trans. Antennas Propag.*, vol. 65, no. 12, pp. 6213–6230, Dec. 2017.

[2] W. Hong, K.-H. Baek, and S. Ko, "Millimeter-wave 5G antennas for smartphones: Overview and experimental demonstration," *IEEE Trans. Antennas Propag.*, vol. 65, no. 12, pp. 6250–6261, Dec. 2017.

[3] W. Hong *et al.*, "Multibeam antenna technologies for 5G wireless communications," *IEEE Trans. Antennas Propag.*, vol. 65, no. 12, pp. 6231–6249, Dec. 2017.

[4] J. Wu, Y. J. Cheng, and Y. Fan, "60-GHz substrate integrated waveguide fed cavity-backed aperture-coupled microstrip patch antenna arrays," *IEEE Trans. Antennas Propag.*, vol. 63, no. 3, pp. 1075–1085, Mar. 2015.

[5] Y. Yu, W. Hong, Z. H. Jiang, and H. Zhang, "E-band low-profile, wideband 45° linearly polarized slot-loaded patch and its array for millimeter-wave communications," *IEEE Trans. Antennas Propag.*, vol. 66, no. 8, pp. 4364–4369, May 2018.

[6] S. Gao, Q. Luo, and F. Zhu, *Circularly Polarized Antennas*. Hoboken, NJ, USA: Wiley, 2014.

[7] X. Bai, S.-W. Qu, S. Yang, J. Hu, and Z.-P. Nie, "Millimeter-wave circularly polarized tapered-elliptical cavity antenna with wide axial-ratio beamwidth," *IEEE Trans. Antennas Propag.*, vol. 64, no. 2, pp. 811–814, Feb. 2016.

[8] Q. Wu, J. Yin, C. Yu, H. Wang, and W. Hong, "Low-profile millimeter-wave SIW cavity-backed dual-band circularly polarized antenna," *IEEE Trans. Antennas Propag.*, vol. 65, no. 12, pp. 7310–7315, Dec. 2017.

[9] J. Zhu, S. Liao, Y. Yang, F. Li, and Q. Xue, "60 GHz dual-circularly polarized planar aperture antenna and array," *IEEE Trans. Antennas Propag.*, vol. 66, no. 2, pp. 1014–1019, Feb. 2018.

[10] J. Wang *et al.*, "Millimeter-wave wideband circularly polarized planar complementary source antenna with endfire radiation," *IEEE Trans. Antennas Propag.*, vol. 66, no. 7, pp. 3317–3326, Jul. 2018.

[11] M. Li and K.-M. Luk, "A wideband circularly polarized antenna for microwave and millimeter-wave applications," *IEEE Trans. Antennas Propag.*, vol. 62, no. 4, pp. 1872–1879, Apr. 2014.

[12] Y. Li, Z. N. Chen, X. Qing, Z. Zhang, J. Xu, and Z. Feng, "Axial ratio bandwidth enhancement of 60-GHz substrate integrated waveguide-fed circularly polarized LTCC antenna array," *IEEE Trans. Antennas Propag.*, vol. 60, no. 10, pp. 4619–4626, Oct. 2012.

[13] C. Liu, Y.-X. Guo, X. Bao, and S.-Q. Xiao, "60-GHz LTCC integrated circularly polarized helical antenna array," *IEEE Trans. Antennas Propag.*, vol. 60, no. 3, pp. 1329–1335, Mar. 2012.

[14] J. Wu, Y. J. Cheng, and Y. Fan, "Millimeter-wave wideband high-efficiency circularly polarized planar array antenna," *IEEE Trans. Antennas Propag.*, vol. 64, no. 2, pp. 535–542, Feb. 2016.

[15] Y. Li and K.-M. Luk, "A 60-GHz wideband circularly polarized aperture-coupled magneto-electric dipole antenna array," *IEEE Trans. Antennas Propag.*, vol. 64, no. 4, pp. 1325–1333, Apr. 2016.

[16] Q. Zhu, K.-B. Ng, and C. H. Chan, "Printed circularly polarized spiral antenna array for millimeter-wave applications," *IEEE Trans. Antennas Propag.*, vol. 65, no. 2, pp. 636–643, Feb. 2017.

[17] J. Zhu, S. Liao, S. Li, and Q. Xue, "60 GHz wideband high-gain circularly polarized antenna array with substrate integrated cavity excitation," *IEEE Antennas Wireless Propag. Lett.*, vol. 17, no. 5, pp. 751–755, May 2018.

[18] H. Xu, J. Zhou, K. Zhou, Q. Wu, Z. Yu, and W. Hong, "Planar wideband circularly polarized cavity-backed stacked patch antenna array for millimeter-wave applications," *IEEE Trans. Antennas Propag.*, vol. 66, no. 10, pp. 5170–5179, Oct. 2018.

[19] Q. Wu, J. Hirokawa, J. Yin, C. Yu, H. Wang, and W. Hong, "Millimeter-wave planar broadband circularly polarized antenna array using stacked curl elements," *IEEE Trans. Antennas Propag.*, vol. 65, no. 12, pp. 7052–7062, Dec. 2017.

[20] L. Zhang, S. Gao, Q. Luo, P. R. Young, W. Li, and Q. Li, "Inverted-S antenna with wideband circular polarization and wide axial ratio beamwidth," *IEEE Trans. Antennas Propag.*, vol. 65, no. 4, pp. 1740–1748, Apr. 2017.